

Luminescent Solar Concentrators for Fibre Optic Daylighting

Alan Arthur Earp
BSc App Phys (Hons)

Department of Applied Physics
University of Technology, Sydney
Australia

A thesis submitted for the Degree of Doctor of Philosophy

June 2005,

Resubmitted with revisions

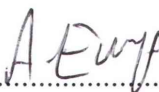
February 2006

CERTIFICATE

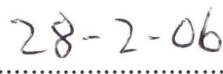
I certify that this thesis has not already been submitted for any degree and is not being submitted as part of the candidature of any other degree.

I also certify that the thesis has been written by me and that any help I have received in preparing this thesis, and all sources used, have been acknowledged in this thesis

Signature of Candidate

.....


Alan Arthur Earp

.....


Date

Acknowledgements

I am deeply grateful to my supervisor, Prof. Geoff Smith, for his guidance during the course of this work, and for his assistance in editing and ensuring the physical correctness of all published work.

I would like to thank my co-supervisor, Jim Franklin, for his technical insight and constant support during the multitude of challenges encountered in this work, as well as his dedication to proofreading and editing my publications and thesis chapters.

Many thanks are due to Paul Swift for his support and technical supervision during the early stages of my candidature, and for passing on and explaining the LSC stack model that laid the foundation for the theoretical work.

I would also like to thank Chris Deller for her co-operation and collaboration at various stages of the project – particularly regarding the modelling of TRIMM diffuser particles. Your assistance was much appreciated.

To my wife, Catherine, I wish to convey sincere thanks for putting up with my ‘tunnel vision’ approach to getting my thesis finished. Your patience and support were much appreciated and they have finally paid off – I finished the thesis!

Thanks are also due to the anonymous journal referees who provided useful comments on the white paint BRDF work in chapter 8, making it more robust.

Finally, I wish to acknowledge the funding of an Australian Postgraduate Award and stipend from the Australian Commonwealth Government, which provided the financial backing required to enable me to undertake this research full-time.

Author's Publications

Journal Publications

Earp, A.A., Smith, G.B., Swift, P.D., Franklin, J. (2004).

Maximising the Light Output of a Luminescent Solar Collector.

Solar Energy 76 (6), 655-667.

Earp, A.A., Smith, G.B., Swift, P.D., Franklin, J. (2004).

Optimisation of a three-colour luminescent solar concentrator daylighting system

Solar Energy Materials and Solar Cells 84, 411-426.

Smith, G.B., Earp, A., Franklin, J., McCreddie, G. (2001).

Novel high performance scattering materials for use in energy saving light fittings and skylights based on polymer pigmented with polymer.

Proceedings of SPIE solar and switchable materials, San Diego, CA, United States, pp. 10-18.

Earp, A.A., Smith, G. B. and Franklin, J.

BRDF of a Non-Lambertian diffuse surface at arbitrary angles of incidence

Lighting Research and Technology (submitted Dec. 2004, publication pending)

Conference Proceedings

Earp, A.A., Smith, G.B., Franklin, J. (2005). Extraction of trapped light from luminescent solar concentrators. *Proceedings of AIP Congress*, ANU, Canberra, pp. 104-107 AIP.

Abstract

Daylight is an abundant source of energy that, if used effectively for lighting in buildings, can improve quality of life and decrease the demand for electric lighting and air-conditioning, reducing energy consumption and costs. Various daylighting systems are available for daylighting the perimeter zones of buildings. However, it is more difficult to transport daylight to remote rooms. The few systems available for remote room daylighting are expensive or disruptive to the building design and rely heavily on direct sunlight.

Luminescent Solar Concentrators (LSC's) contain fluorescent dyes that absorb both direct and diffuse sunlight without tracking the sun, causing fluorescent emission in a specific wavelength range. LSC's can potentially be used for daylighting, but the only previously demonstrated system is rather bulky and architecturally intrusive, and its output is yellow-green and difficult to control. A stack of three coloured LSC's is proposed in this thesis, which produces a good white output of over 1,000 lumens under solar illumination of 100,000 lux. This output is transported to a remote room in narrow flexible polymer light guides.

A theoretical model of the three-colour LSC stack was developed, which uses the absorption and emission spectra of the dyes to predict the LSC's output spectrum and lumens. Studies with this model revealed the importance of highly accurate absorption tails data for good prediction of the stack performance. The model was used to determine the optimum size and dye concentration for each LSC. A simple experimental method was devised for characterising the optical performance of a fixed size LSC.

Half of the emitted light is trapped at the end of the light guides, so a 'light extractor' is required to enable this light to escape. Ray tracing simulations were carried out for various light extractor designs, from which the optimal light extractor size, shape and configuration were determined for maximum optical gain. With a good light extractor design, a gain of 1.7-1.8 should be achievable, but with the current prototypes, the gain is limited to 1.2-1.3, limiting the output to around 1,100 lumens. The violet collector sheet in the LSC stack was also found to be problematic, so an alternative blue light source is proposed. Hence there is room for improvement in future prototypes.

Table of Contents

Acknowledgements	iii
Author's Publications	iv
Abstract	v
Table of Contents.....	vi
List of Figures.....	x
List of Tables	xvii
List of Symbols Used.....	xix
1 Introduction/Overview	1
1.1 Summary of Motivations Behind Study	1
1.2 Thesis outline	2
2 Motivations for Development of a Novel Daylighting System	5
2.1 Abundance of Solar Energy	5
2.2 Benefits of Daylight.....	6
2.2.1 Colour Rendering	6
2.2.2 Natural Variability.....	6
2.2.3 High Luminous Efficacy.....	7
2.2.4 Reduction in Energy Usage.....	8
2.2.5 Health and Productivity	8
2.3 Background Science and Technology	9
2.3.1 Daylighting	9
2.4 Luminescent Solar Concentrators for Daylighting.....	17
2.5 Conclusions	20
3 Three Colour Luminescent Solar Concentrator Stack Overview .	23
3.1 Three Colour LSC Stack.....	23
3.1.1 LSC Stack Design.....	23
3.1.2 Stack Modelling Theory	26
3.2 Conclusions	30
4 Maximising the Light Output of a Luminescent Solar Concentrator.....	31
4.1 Introduction	31
4.2 Light Transport Performance	34
4.2.1 Assessing Sheet Quality for Lighting	34
4.2.2 Measurement of $L_{1/2}$	35
4.2.3 Theoretical Calculation of $L_{1/2}$	35
4.2.4 Experimental and Theoretical $L_{1/2}$ Results.....	38
4.3 Separating Dye and matrix effects.....	40
4.3.1 Dye-Related Losses	41
4.3.2 Effect of Dye Residual Attenuation.....	42
4.3.3 Matrix-Related Losses.....	44
4.4 Optimisation of Collector properties	45
4.5 Conclusions	49

5	Absorption and Emission Measurements	51
5.1	Introduction	51
5.2	Absorption.....	51
5.2.1	Cary Spectrophotometer	53
5.2.2	UTS High-Precision Spectrophotometer	58
5.2.3	Combining the Two Transmission Data Sets.....	62
5.3	Emission.....	64
5.3.1	Excitation Wavelength	64
5.3.2	Absorption & Emission Overlap	66
5.4	Conclusions	67
6	Spectral Properties of Three-Layer LSC.....	70
6.1	Introduction	70
6.2	Incident Energy.....	70
6.2.1	Transmitted Component.....	70
6.2.2	Reflected Component	72
6.2.3	Emitted Component	73
6.2.4	Total Incident Energy.....	73
6.3	Absorbed Energy.....	75
6.3.1	UV-Blocking Cover Sheet	77
6.4	Conclusions	79
7	Extraction of Trapped Light	81
7.1	Introduction	81
7.1.1	Trapped Light vs. Endlight	81
7.1.2	Fresnel Reflection Coefficient	84
7.1.3	Trapped Light-Endlight Ratio.....	86
7.2	Effect of Dye Attenuation on Trapped Light	87
7.2.1	Simulation of Trapped Light-Endlight Ratio.....	87
7.2.2	Weighted Mean Trapped Light-Endlight Ratio.....	92
7.2.3	Weighted Mean Fresnel Reflection Coefficient	94
7.3	Extraction of Trapped Light	96
7.3.1	The Role of the Light Extractor.....	96
7.3.2	Assessing the Performance of a Light Extractor.....	98
7.4	Conclusions	100
8	Bi-Directional Reflectance of Diffuse White Paint at Arbitrary Angles of Incidence	101
8.1	Introduction	101
8.2	Measurement of BRDF	103
8.2.1	Sample and BRDF Measurement Geometry.....	103
8.2.2	Effect of Surface Finish on BRDF	106
8.2.3	Effect of Surrounding Medium on BRDF	108
8.2.4	Pseudo-Specular Reflectance	109
8.3	Two-Component BRDF Model	110
8.3.1	Distinguishing Between Pseudo-Specular and Lambertian Reflectance	110
8.3.2	Fitting a Function to the Pseudo-Specular Peaks.....	111
8.3.3	Comparison with Measured Data	115
8.3.4	Probability of Diffuse Reflection.....	116
8.4	Conclusions	119

9	Monte Carlo Light Extractor Ray Tracing Simulations.....	121
9.1	Introduction	121
9.1.1	Simulation Outline	121
9.2	Reflection from the Diffuse White Surface.....	123
9.2.1	Simulation of Reflection.....	123
9.2.2	Magnitude of Reflectivity	123
9.2.3	Reflection Type.....	125
9.2.4	Pseudo-Specular Frame of Reference.....	125
9.2.5	Distribution of Pseudo-Specular Rays	127
9.2.6	Reducing Simulation Time.....	132
9.3	Microsphere Deviation.....	132
9.3.1	Average Distance Between Microspheres	133
9.3.2	Angular Deviation from Microspheres	134
9.4	Conclusions	136
10	Light Extractor Simulation Results	137
10.1	Introduction	137
10.2	V-Groove Light Extractor	138
10.3	Bevelled Edge Light Extractors.....	139
10.3.1	Varying Height	140
10.3.2	Doping with Microspheres	141
10.4	Rectangular Light Extractors.....	142
10.4.1	Paint Reflectivity	143
10.4.2	Number of Edges Painted	144
10.4.3	Uniform TRIMM-Doping.....	149
10.4.4	Choosing Optimal Dimensions	150
10.5	Conclusions	154
11	Performance Issues for Practical LSC Stack Systems.....	156
11.1	Introduction	156
11.2	Individual LSC Sheets	156
11.2.1	Surface Flatness	157
11.2.2	Clean Surfaces	158
11.2.3	Polished Edges	160
11.2.4	Complete Dissolution of Dye.....	162
11.2.5	Excellent Optical Joints	164
11.3	Three-Layer LSC	167
11.3.1	Collector	167
11.3.2	Light Guides	168
11.3.3	Light Extractor	170
11.4	Conclusions	171
12	LSC Stack Output Properties	173
12.1	Introduction	173
12.2	Measurement Process	173
12.2.1	Calibration	173
12.2.2	Spectral Correction.....	175
12.3	Luminous Output.....	178
12.3.1	Measurements vs. Model	178
12.3.2	Quality of Optical Joints	181
12.4	Output Colour	183

12.5	Conclusions	186
13	Future Work and Other Applications of LSC's	188
13.1	Introduction	188
13.2	Improving 'Blue' Light Source of Three-Layer LSC	189
13.2.1	Theoretical Blue Fluorescent Dye	190
13.2.2	Blue LED.....	191
13.3	Hybrid PV-LED/LSC Stack.....	193
13.4	Improving the Light Guides.....	194
13.4.1	Narrow 'Ribbon' Light Guides	194
13.4.2	Optic Fibre Light Guides	195
13.5	24-hr Lighting System	196
13.6	Other Applications of LSC's: Luminescent Pixels	197
13.7	Conclusions	200
14	Conclusions	202
14.1	Research Need.....	202
14.2	Optimisation of Collector Properties.....	202
14.3	Absorption & emission.....	203
14.4	LSC Stack Spectral Properties	204
14.5	Trapped Light.....	205
14.6	White Paint BRDF.....	205
14.7	Light Extractor Simulation Results	206
14.8	Light Output Properties	208
	Appendix	210
	References.....	213

List of Figures

Figure 1.1 – General operating principle of a Luminescent Solar Concentrator (LSC).....	2
Figure 2.1 – A thermotropic layer is transparent at low temperatures, but blocks heat and direct sunlight at high temperatures (Georg, Graf et al. 1998). Thermotropic windows help reduce thermal gain and loss, reducing cooling loads. This improves thermal comfort in winter, but can trap some heat inside on summer evenings, reducing thermal comfort.	11
Figure 2.2 – Horizontal light pipes (Chirarattananon, Chedsiri et al. 2000) bring daylight into interior rooms from a façade. Due to the structural nature of these light pipes, they must be introduced during the building design stage – retrofitting is very difficult.....	14
Figure 2.3 –A tubular light pipe directs light down to a diffuser at the base. These light pipes are quite bulky, with diameters of 250 – 400 mm, making it difficult to extend them to lower floors. Furthermore, the highly reflective material required is expensive, making it a less attractive option for long light pipes.	14
Figure 2.4 – Natural illumination of a cellar with a heliostat and mirrors (Pohl and Anslem 2002). These systems are effective, but require complex tracking and focussing systems, making them expensive to implement.....	15
Figure 2.5 – Hybrid daylight/artificial light system utilising a tracking solar concentrator and optic fibres (Schlegel, Burkholder et al. 2004). The tracking concentrator collects sunlight and concentrates it onto a collection of optical fibres, which distribute it to remote rooms. The luminaires have built-in artificial lights as backup for when daylight availability is low.....	17
Figure 2.6 – Remote room daylighting systems (Zastrow & Wittwer, 1986) using mirror light pipes (left) and fluorescent solar collectors (right). In the fluorescent system, daylight is collected at the top with a conical collector; fluorescent emission is transmitted 6.5 m through a transparent PMMA light pipe. The output is reflected into a room with a mirror, providing significant improvements to the light level in the room.	19
Figure 2.7 – Proposed new three-colour Luminescent Solar Concentrator daylighting system. Sunlight is collected at the roof with a three-layer LSC stack, and the emitted light is directed into a remote room via transparent flexible polymer light guides (coated in black protective film in diagram). A light extractor at the far end extracts trapped light, boosting the output at the luminaire.....	20
Figure 3.1 - Schematic of a three-colour LSC stack connected to light guides and light extractor	23

Figure 3.2 - Extraction of trapped light - (a) Without a light extractor, half of the light at the end of the light guide is trapped, (b) The light extractor enables much of the trapped light to escape	24
Figure 3.3 - Luminescent Solar Concentrator of length L , illuminated by source $S(\mathcal{Y})$, produces end emission $\epsilon(\lambda, L)$ at collection edge.	27
Figure 3.4 - Absorption and incident energy spectra for 50 ppm pink sheet at the bottom of a three-colour LSC stack on a base reflector	29
Figure 3.5 – Measured output spectra due to Stokes shift and modelled self-absorption shifts for two length values with fluorescent pink dye.....	30
Figure 4.1 - Absorption and emission spectra of green fluorescent dye at 60ppm.....	33
Figure 4.2 - Experimental setup for measurement of the half-length of an LSC.	36
Figure 4.3 - Luminous output as a function of length for a 1.2 m, 60 ppm green LSC. Here a perfect non-scattering matrix is compared with a standard matrix with a matrix half-length $L_{m^{1/2}} = 5$ m, and the slope δ is given in two separate regions; $0.4 \text{ m} < l < 0.9 \text{ m}$ and $1.0 \text{ m} < l < 2.0 \text{ m}$	39
Figure 4.4 - Transmission tails of Green LSC (dye only) The solid line represents the measured transmission of the green dye (excluding Fresnel reflectance), and the dashed line is the same spectrum, except that the transmission in the ‘tails region’ beyond 520 nm has been artificially set to 100% (shown as a reference).	42
Figure 4.5 - Effect of residual dye attenuation factor β on concentration dependence of output of pink dyed sheet	44
Figure 4.6 - Theoretical half-length for a 1.2 m green LSC as a function of dye concentration, for a perfect non-scattering matrix with no tails attenuation (-----), a perfect non-scattering matrix with measured tails attenuation (——), a standard matrix ($L_{m^{1/2}} = 5$ m) with 100% dye transmission in the tails region (----) and a standard matrix with measured tails attenuation (— — — —).....	45
Figure 4.7 - Theoretical luminous output as a function of dye concentration for a 1.2 m green LSC- for a perfect non-scattering matrix with no tails (-----), a perfect non-scattering matrix with measured tails attenuation (——), a standard matrix ($L_{m^{1/2}} = 5$ m) with 100% dye transmission in the tails region (----) and a standard matrix with measured tails attenuation (— — — —).....	46
Figure 4.8 - Theoretical luminous output vs. collector length for a green LSC with fluorescent dye at concentrations of 30 ppm, 60 ppm and 100 ppm in (a) a standard matrix of half-length $L_{m^{1/2}} = 5$ m and (b) a perfect non-scattering matrix	48
Figure 4.9 - Theoretical light-to-light efficiency vs. collector length for a green LSC with fluorescent dye at concentrations of 30 ppm, 60	

ppm and 100 ppm in (a) a standard matrix of half-length $L_{m^{1/2}} = 5$ m and (b) a perfect non-scattering matrix	49
Figure 5.1 - Transmission of 60 ppm green fluorescent dye over 2 mm from two reference measurements in Cary spectrophotometer.	53
Figure 5.2 – 100% transmission signal of Cary spectrophotometer.	54
Figure 5.3 –Ratio of transmission spectra of pairs of glass and quartz cuvettes	55
Figure 5.4 –Transmission of green fluorescent dye scaled to a 2 mm path length at various concentrations in MMA as measured by diluting a master solution in a quartz cuvette with the Cary spectrophotometer.....	56
Figure 5.5 – Dye attenuation coefficient, $\alpha(\lambda)$, from transmission data of dye at multiple concentrations in MMA.....	57
Figure 5.6 - Schematic of McCredie Spectrophotometer when set up for transmission measurements	58
Figure 5.7 – 16 mm samples for accurate tails transmission measurements with the McCredie spectrometer	59
Figure 5.8 - Transmission of 16 mm samples (from the McCredie spectrometer).....	59
Figure 5.9 – Impact of fluorescence on dye transmission of 16 mm samples, measured with Cary and McCredie spectrophotometers for three dyes; (a) green 60 ppm, (b) pink 50 ppm, (c) violet 120 ppm.....	60
Figure 5.10 - Equivalent tails transmission of 2 mm LSC samples (from McCredie and Cary Spectrometers)	62
Figure 5.11 - Transmission of 2 mm samples: (a) absorption region from Cary spectrometer and (b) tails region from McCredie spectrometer	63
Figure 5.12 – Relative emission intensity vs. excitation wavelength for a 60 ppm green LSC sample	65
Figure 5.13 – Relative emission intensity for the violet, green and pink dyes	66
Figure 5.14 – Overlap of emission and absorption spectra for (a) 60 ppm green, (b) 50 ppm pink dyes, and (c) 120 ppm violet.....	67
Figure 5.15 – Dye emission and LSC output emission for (a)60 ppm green, (b) 50 ppm pink and (c) 120 ppm violet LSC sheets of length 1.2 m	68
Figure 6.1 – Incident energy distribution for each LSC in three-layer stack	71
Figure 6.2 – Transmitted energy spectra for each LSC sheet in three- layer stack	72
Figure 6.3 - Incident energy components for the various LSC's in a three-layer LSC stack; (a) violet, (b) green and (c) pink.....	74

Figure 6.4 – Total incident energy spectra for the various LSC's in a three-layer LSC stack; (a) violet, (b) green and (c) pink.....	75
Figure 6.5 – Total absorbed energy spectra for violet, green and pink LSCs in three-layer stack	76
Figure 6.6 – Absorption overlap of violet LSC and UV-blocking cover sheet	77
Figure 6.7 – Total absorbed energy with and without the cover sheet for the various LSCs (a) violet, (b) green and (c) pink.....	79
Figure 7.1 – (a) Endlight can pass through an end surface and (b) trapped light is totally internally reflected at all surfaces.....	82
Figure 7.2 - Distribution of emitted light from a dye molecule within a LSC sheet (loss cones 5 and 6 have been omitted for clarity).....	83
Figure 7.3 – Fresnel reflectance coefficients for an interface between PMMA ($n_2 = 1.495$) and air ($n_1 = 1.000$)	85
Figure 7.4 - LSC sheet geometry for trapped light simulation	89
Figure 7.5 – Flowchart of the simulation used to calculate the ratio of trapped light to endlight at the end of the light guide, assuming no re-emission occurs.....	91
Figure 7.6 – Simulation of trapped light and endlight fractions, 100 simulations of 10,000 rays each	92
Figure 7.7 – Attenuated trapped light-endlight ratio $F_{at}(\lambda, L)$, sheet output emission spectrum $\epsilon(\lambda, L)$, initial trapped light-endlight ratio F_o , and weighted mean attenuated trapped light-endlight ratio \bar{F}_{at} for violet, green and pink LSC sheets of length 1.2 m.....	93
Figure 7.8 – Transmission of dyes over 1.2 m LSC sheet	93
Figure 7.9 - Extraction of trapped light: (a) without a light extractor, up to half of the light in the light guide of thickness t is trapped. (b) a light extractor enlarges the exit aperture by height h and depth d , enabling extraction of trapped light	97
Figure 8.1 - Variation of reflectance profile with angle: (a) Lambertian reflection at low angles of incidence and (b) pseudo-specular reflection at high angles of incidence	102
Figure 8.2 – Photogoniometer measurement geometry for bidirectional reflectance function (BRDF)	105
Figure 8.3 – Various surfaces investigated for angular reflectance: (a) smooth clear, (b) smooth white, (c) rough clear and (d) rough white.....	106
Figure 8.4 – In-plane BRDF for various surface finishes and angles of incidence	107
Figure 8.5 – In-plane BRDF for a diffuse white surface at various angles of incidence, facing air ($n=1.0$) and facing PMMA ($n=1.495$)	108
Figure 8.6 – In-plane BRDF of a white rough surface behind PMMA at high angles of incidence.....	109

Figure 8.7 – Pseudo-specular component of in-plane BRDF as a function of angle of incidence.....	111
Figure 8.8 - Lorentzian width and amplitude parameters for pseudo-specular reflectance as a function of angle of incidence	114
Figure 8.9 - Lorentzian peak angle parameter, θ_o , as a function of angle of incidence	114
Figure 8.10 - Lorentzian fits to $BRDF_{PS}(\theta_i, \gamma)$, multiplied by $\cos \gamma$; measured pseudo-specular components (solid lines) and modelled Lorentzian curves (dashed lines).....	116
Figure 8.11 - Measured and modelled in-plane $BRDF_{Total}(\theta_i, \gamma)$ multiplied by $\cos \gamma$; measured (solid lines), diffuse component (dotted lines), pseudo-specular component (dashed lines) and total modelled BRDF (dot-dashed lines).....	117
Figure 8.12 - Probabilities of diffuse and pseudo-specular reflection, $P_D(\theta_i)$ and $P_{PS}(\theta_i)$ respectively, from diffuse white paint behind PMMA. $P_D(\theta_i)$ has also been fitted with a Gaussian curve.....	119
Figure 9.1 - Simulation of a ray path in a light extractor with all edges and the back surface painted with diffuse white paint	122
Figure 9.2 - Reflection algorithm for diffuse white paint on edges of a rectangular light extractor	124
Figure 9.3 - Probability of diffuse reflection from a white paint surface. ..	125
Figure 9.4 - Reflectance of 'One Stroke White' diffuse white paint, measured with three different integrating spheres.....	125
Figure 9.5 - Original axes used in light extractor simulations, and the local axes for an example pseudo-specular reflected ray.....	126
Figure 9.6 - Normalised Lorentzian pseudo-specular reflectance scattering function, $L(\theta, \gamma)$, for multiple angles of incidence.....	128
Figure 9.7 - Weighted Lorentzian pseudo-specular reflectance scattering probability function, $L(\theta, \gamma)P_{PS}(\theta)$, for multiple angles of incidence	129
Figure 9.8 – Maximum limit for deviation co-ordinates x' and y' , as a function of angle of incidence.....	130
Figure 9.9 - Minimum limit for z' co-ordinate as a function of angle of incidence	131
Figure 9.10 - Two-dimensional microsphere deviation geometry	134
Figure 9.11 - Three-dimensional spherical trigonometry for refraction from a microsphere.....	135
Figure 10.1 - V-Groove light extractor design.....	139
Figure 10.2 - Bevelled edge light extractor design.....	140
Figure 10.3 - Simulation results for bevelled edge light extractor as a function of height (10,000 rays, $W = 25t$, $D = t$, $t = 6$ mm).....	141

Figure 10.4 – Geometry of a light extractor connected to a stack of three light guides	142
Figure 10.5 - Simulation results for a rectangular light extractor ($H = 5t$, $W = 25t$) with paint on all edges, for multiple paint reflectance values	143
Figure 10.6 – Light distribution from ceiling-mounted rectangular light extractors with (a) paint on back surface only; (b) paint on all edges.....	144
Figure 10.7 – Simulation results for rectangular light extractors with no diffuser, with various surfaces painted. ($D = 2t$, $W = 25t$, $H = 8.3t$, $t = 6\text{mm}$, 10,000 rays per simulation)	145
Figure 10.8 - Cross-section of a light extractor with a TRIMM diffuser sheet	146
Figure 10.9 - Simulation results for rectangular light extractors with a TRIMM diffuser sheet, and various surfaces painted. ($D = 1.5t$, $D_{\text{TRIMM}} = 0.5t$, $W = 25t$, $H = 8.3t$, $t = 6\text{mm}$, 10,000 rays per simulation).....	147
Figure 10.10 - Simulation results for a rectangular light extractor with paint on back and ends, doped throughout with various microsphere concentrations. The dimensions are $D = 1.67t$, $H = 7.5t$, $W = 25t$	149
Figure 10.11 - Variation of light output with height, for a rectangular light extractor with all edges painted	151
Figure 11.1 – Transport losses in LSC sheets: (a) flat parallel surfaces totally internally reflect all rays travelling at or above the critical angle, χ ; (b) thickness variation causes ray at angle $\chi_2 > \chi$ to totally internally reflect, while critical angle ray escapes, leading to additional light loss.....	157
Figure 11.2 – These LSC sheets have thickness variations of 6% of the nominal thickness of $t = 2.0\text{ mm}$, causing up to 8% light loss when connected to a light guide	158
Figure 11.3 –Additional transport losses in LSC sheets: (a) flat parallel surfaces totally internally reflect all rays travelling at or above the critical angle; (b) dirt and scratches enable light at or above the critical angle to escape, causing additional light loss.....	159
Figure 11.4 - LSC sample design used to measure light extractor gain. Light output is measured at each end separately with an integrating sphere (omitted for clarity). The black tape is placed on the right hand side of the lamp to measure I_{end} , and on the left hand side to measure I_{le}	165
Figure 11.5 – Cross-section of cover sheet on LSC stack	168
Figure 11.6 – Reinforcing the optical joint between the collector sheets and the light guides.....	169
Figure 11.7 –External layers to protect light guide from dust, scratches and stray light (cross-section)	170

Figure 11.8 – Light extractor and light guide dimensions for prototype LSC stack.....	171
Figure 12.1 – Measurement of luminous output of LSC sheets under solar illumination.....	174
Figure 12.2 – Measuring lux to lumens conversion factor for integrating sphere.....	174
Figure 12.3 – Integrating sphere masks with two slit sizes (a) for individual LSC's or stack without light extractor, and (b) for LSC's with a light extractor installed.....	175
Figure 12.4 – Measuring the spectral response of the white reflective surface inside an integrating sphere.	176
Figure 12.5 – LSC emission spectra overlaid with the weighted spectral response of the integrating sphere, $R_{sph}(\lambda)$, and the human eye, $V(\lambda)$	177
Figure 12.6 - Output spectrum of the three-colour LSC stack.....	184
Figure 12.7 - CIE 1973 colour co-ordinates of the output of pink, green & violet sheets and the LSC stack.....	185
Figure 13.1 – Absorption and emission spectra of violet fluorescent dye, overlaid with absorption of cover sheet and eye's photopic response	189
Figure 13.2 – Absorption and emission spectra of hypothetical blue fluorescent dye, overlaid with absorption of cover sheet and eye's photopic response.....	190
Figure 13.3 – Simulated output of two-layer LSC stack with 15 blue LEDs, overlaid with eye's photopic response.....	192
Figure 13.4 - Hybrid LED/LSC daylighting system with blue LED powered by a solar cell.....	193
Figure 13.5 – Schematic of a backlit large screen LCD display using luminescent solar concentrators	197
Figure 13.6 – Fractions of emitted rays from luminescent pixels escaping at each surface, with various diffusing elements. The pixel is simultaneously backlit and illuminated from the front.....	198
Figure 13.7 – A luminescent pixel with its back surface partially painted with diffuse white paint, to allow for three lighting modes: (a) sunlight only, (b) backlight only and (c) both sunlight and backlight.....	199

List of Tables

Table 2-1 – Comparison of various daylighting systems	21
Table 4-1 - Theoretical and experimental LSC half-length, $L_{1/2}$ (in metres), for a 60 ppm green LSC with dimensions 1.20 m x 0.135 m x 0.002 m. Results are shown for both a standard matrix ($L_{m1/2} = 5$ m) and a simulated perfect non-scattering matrix ($L_{m1/2} \sim \infty$).....	40
Table 4-2 - Effect of attenuation factor β on half-length and luminous output of 2 mm thick 120 ppm violet, 50 ppm pink and 60 ppm green sheets (without a light extractor).....	43
Table 5-1 - Emission wavelength measurement range and excitation wavelength λ for the violet, green and pink fluorescent Lumogen dyes used in this work.	65
Table 6-1 - Absorbed energy calculated for violet, green and pink LSCs in a three-layer stack, with and without a UV-blocking cover sheet.....	78
Table 7-1 – Mean trapped light and endlight fractions at the end of a 1.2 m LSC sheet, and their ratio \bar{F}_{at} , weighted over the emission region of each dye.	94
Table 7-2 – Simulated weighted mean Fresnel reflectance coefficients and endlight extraction efficiencies of a polished LSC end, without dye attenuation and for each 1.2 m LSC	96
Table 7-3 – Overall efficiency of a polished light guide end, without dye attenuation and at the end of each 1.2 m LSC	99
Table 7-4 – Practical maximum overall efficiency gain for a high-quality light extractor ($\eta_{end} = 0.98$ & $\eta_{trap} = 0.85$) on 1.2 m-long violet, green and pink LSC sheets.	100
Table 10-1 - Simulation results for a rectangular light extractor (10,000 rays, $D = 2t$, $H = 7.5t$, $W = 25t$), with and without a light extractor.	139
Table 10-2 – Simulation results for a bevelled edge light extractor with and without microspheres (10,000 rays, $W = 25t$, $D = t$, $H = 10t$)	141
Table 10-3 - Extraction efficiencies and gain for rectangular light extractors with various painted edges, with and without a diffuser on a 60 ppm green LSC.....	148
Table 10-4 – Simulation results for a rectangular light extractor with dimensions $H = 7.5t$, $W = 25t$ and multiple depth values.....	153
Table 11-1 – Summary of different methods used to clean LSC sheets	159
Table 11-2 - Variation of half-length with LSC edge quality	161
Table 11-3 – Effect of undissolved dye on LSC appearance and half-length ..	162
Table 11-4 - Measured and simulated gain values for a range of light extractors.....	166
Table 12-1 - Dimensions of slits in integrating sphere masks for luminous output measurements	175

Table 12-2 - Spectral correction factor, K , for luminous flux measurements of each LSC with 300 mm integrating sphere.	178
Table 12-3 – Measured & Modelled Luminous output of LSC's (without light guides) normalised to 100,000 lux solar illumination	179
Table 12-4 - Luminous output and light-to-light efficiency of three-layer stack at various stages of production, normalised to a solar illumination of 100,000 lux	183
Table 13-1 - Outputs of violet LSC and 'hypothetical blue LSC' on top layer of three-layer LSC stack with UV-blocking cover sheet	191

List of Symbols Used

Symbol	Description	Units
$\alpha(\lambda)$	Wavelength-dependent attenuation coefficient of fluorescent dye	m^{-1}
α_m	Attenuation coefficient of polymer matrix (assumed to be wavelength independent)	m^{-1}
$A(\lambda)$	Absorption spectrum of fluorescent dye	
$A(\theta_i)$	Area of pseudo-specular beam as a function of angle of incidence	
A_{det}	Area of detector in photogoniometer	m^2
β	Artificial dye tails attenuation factor (for studying effect of reduced tails attenuation on LSC performance)	
$BRDF(\theta_i, \gamma, \omega)$	Bi-directional Reflectance Distribution Function of white diffuse surface inside light extractor (three-dimensional)	sr^{-1}
$BRDF(\theta_i, \gamma)$ or $BRDF(\theta_i, \gamma)_{Total}$	Bi-directional Reflectance Distribution Function of white diffuse surface inside light extractor (two-dimensional)	sr^{-1}
$BRDF_D(\theta_i, \gamma)$	Diffuse component of two-dimensional BRDF	sr^{-1}
$BRDF_{PS}(\theta_i, \gamma)$	Pseudo-specular component of two-dimensional BRDF	sr^{-1}
χ	Critical angle of reflection from polymer surface	radians
δ	Exponential loss coefficient: taken from slope of output intensity vs. distance; used to calculate half-length $L_{1/2}$	m^{-1}
σ	Deviation angle caused by a single microsphere	radians
$\varepsilon_o(\lambda)$	Emission spectrum of dye molecule	$\text{W.m}^{-2}.\text{nm}^{-1}$
$\varepsilon(\lambda, L)$	Emission spectrum reaching the end of a LSC of length L	$\text{W.m}^{-2}.\text{nm}^{-1}$
$\varepsilon_V(\lambda)$	Emission spectrum of violet dye	$\text{W.m}^{-2}.\text{nm}^{-1}$
$\varepsilon_G(\lambda)$	Emission spectrum of green dye	$\text{W.m}^{-2}.\text{nm}^{-1}$
$\varepsilon_P(\lambda)$	Emission spectrum of pink dye	$\text{W.m}^{-2}.\text{nm}^{-1}$
$E_{abs}(\lambda)$	Energy absorbed by dye molecules	$\text{W.m}^{-2}.\text{nm}^{-1}$
E_e	Total power emitted by dye molecules	W.nm^{-1}
$E_{VT}(\lambda), E_{GT}(\lambda), E_{PT}(\lambda)$	Transmitted solar energy incident on the violet, green and pink sheets respectively	$\text{W.m}^{-2}.\text{nm}^{-1}$

Symbol	Description	Units
$E_{VR}(\lambda),$ $E_{GR}(\lambda), E_{PR}(\lambda)$	Solar energy reflected from the white base of the stack, incident on the violet, green and pink sheets respectively	$\text{W.m}^{-2}.\text{nm}^{-1}$
$E_{GE}(\lambda)$	Emitted energy from the violet sheet, incident on the green sheet	$\text{W.m}^{-2}.\text{nm}^{-1}$
$E_{PE}(\lambda)$	Emitted energy from the green sheet, incident on the pink sheet	$\text{W.m}^{-2}.\text{nm}^{-1}$
F_o	Ratio of trapped light to endlight at point of dye emission	
F_t	Fraction of emitted rays that are trapped (outside all critical loss cones)	
F_e	Fraction of emitted rays within the critical angle loss cones with respect to the collection edge or mirror edge of the collector	
$F_{at}(\lambda)$	Ratio of trapped light to endlight at end of fixed length collector (varies with wavelength)	
\overline{F}_t	Mean fraction of trapped light at the end of a fixed length collector, weighted over the dye emission region	
\overline{F}_e	Mean fraction of endlight at the end of a fixed length collector, weighted over the dye emission region	
\overline{F}_{at}	Mean ratio of trapped light to endlight at the end of a fixed length collector, weighted over the dye emission region	
Φ_L	Luminous flux at end of uniformly illuminated LSC	lumens
Φ_l	Luminous flux at end surface of LSC when illuminated by a line source at a distance l from end	lumens
Φ_{obs}	Observed luminous flux from end surface of LSC;	lumens
φ	Lux to lumens conversion factor for integrating sphere	
γ	Deviation angle from surface normal in horizontal plane	radians
γ_s	Deviation of reflected ray from specular direction inside light extractor	radians
\overline{G}	Optical gain induced by installation of a light extractor to a collection edge or light guide end, weighted over the emission region of the dye	

Symbol	Description	Units
η_e	Energy-to-energy conversion efficiency of fluorescent dye	
η_{ll}	Light-to-light efficiency of a LSC sheet	
η_q	Quantum efficiency of fluorescent dye	
η_o	<i>Collection edge endlight efficiency</i> ; fraction of light within the critical angle cone with respect to the collection edge that is transmitted on its first pass	
η_{trap}	<i>Light extractor trapped light efficiency</i> ; fraction of trapped light striking front surface of light extractor that is transmitted, on the first or a subsequent pass	
η_{end}	<i>Light extractor endlight efficiency</i> ; fraction of endlight striking front surface of light extractor that is transmitted, on the first or a subsequent pass	
$\bar{\eta}$	<i>Overall light extractor efficiency</i> ; fraction of light entering a light extractor that is transmitted through the front surface	
H	Height of light extractor	m
I_{in}	Incident beam signal in photogoniometer	mV
$I_{ref}(\theta_i, \gamma, \omega)$	Reflected signal from white diffuse surface	mV
I_{end}	Measured signal from output of polished end of LSC, when illuminated by fluorescent lamp a fixed distance from the end	mV
I_{le}	Measured signal from light extractor on end of LSC, when illuminated by fluorescent lamp a fixed distance from the end	mV
I_{sphere}	Illuminance on Hagner photopic detector in integrating sphere when used to measure luminous output of end surface of LSC	lux
I_{sol}	Solar illuminance incident on LSC	lux
K	Mean reflectivity correction factor of integrating sphere interior surface, weighted over dye emission region and photopic response $V(\lambda)$	
$L(\theta_i, \gamma_s)$	Lorentzian function describing direction of pseudo-specular reflected rays, as a function of angle of incidence and deviation from specular direction	
L	Length of fluorescent sheet	m
$L_{d^{1/2}}$	Half-length component from fluorescent dye	m

Symbol	Description	Units
$L_{m/2}$	Half-length component from clear matrix	m
l	Horizontal distance from point of fluorescent emission to end surface of LSC	m
λ	Wavelength of radiation	nm
λ_{exc}	Peak wavelength of excitation beam	nm
ψ	Wavelength of excitation radiation	nm
$\lambda_{min}, \lambda_{max}$	Wavelength limits for emission measurements	nm
LSC	Luminescent Solar Concentrator	
$\langle m \rangle$	Average distance between microspheres	m
$\mu(\theta_i)$	Effective radius of cylinder containing pseudo-specular reflected ray distribution in cylindrical co-ordinates	m
n	Refractive index	
$P_D(\theta_i)$	Probability of diffuse reflection from a white diffuse surface as a function of angle of incidence, θ_i	
$P_{PS}(\theta_i)$	Probability of pseudo-specular reflection from a white diffuse surface as a function of angle of incidence, θ_i	
$P(x)$	Probability of a ray striking a microsphere after travelling a distance x in a TRIMM-doped light extractor or diffuser sheet	
θ	Altitude angle with respect to vertical axis of LSC	radians
ϕ	Azimuthal angle with respect to collection edge of LSC	radians
θ_i	Angle of incidence of ray with respect to surface normal	radians
$\theta_o(\theta_i)$	Pseudo-specular Lorentzian peak-angle parameter as a function of angle of incidence	
$\rho_{DHD}(\theta_i)$	Diffuse component of direct-hemispherical reflectance from white diffuse surface as a function of angle of incidence	
$\rho_{DHPS}(\theta_i)$	Pseudo-specular component of direct-hemispherical reflectance of white diffuse surface as a function of angle of incidence	
r	Radius of rotation of photogoniometer detector	m
R_c	Reflectivity of cover sheet	
R_m	Reflectivity of mirror on back end of collector sheets	

<i>Symbol</i>	<i>Description</i>	<i>Units</i>
$R(\theta_i)$	Radius of pseudo-specular beam as function of angle of incidence	
\bar{R}	Weighted mean Fresnel surface reflectance over critical angle cone at collection edge	
$R_{sph}(\lambda)$	Spectral response of integrating sphere interior surface	
$R_{norm}(\lambda)$	Normalised spectral response of integrating sphere, weighted over dye emission region and photopic response $V(\lambda)$	
$S(\lambda), S(\Psi)$	Solar spectrum incident on fluorescent sheet	$\text{W.m}^{-2}.\text{nm}^{-1}$
t	Thickness of fluorescent sheet	m
$T_{fl}(\lambda)$	Fluorescent component of transmission measurements	
$T_D(\lambda)$	Transmission spectrum of fluorescent dye (excluding Fresnel losses) – generic term	
$T_{LSC}(\lambda)$	Transmission of collector sheet (including Fresnel losses) – generic term	
$T_M(\lambda)$	Transmission of clear polymer matrix (excluding Fresnel losses)	
$T_{Clear}(\lambda)$	Transmission of clear polymer matrix (including Fresnel losses)	
$T_C(\lambda)$	Transmission of cover sheet (including Fresnel losses)	
$T_G(\lambda)$	Transmission of green dye in LSC (excluding Fresnel losses)	
$T_P(\lambda)$	Transmission of pink dye in LSC (excluding Fresnel losses)	
$T_V(\lambda)$	Transmission of violet dye in LSC (excluding Fresnel losses)	
$V(\lambda)$	Photopic response of the human eye	
w	Width of fluorescent sheet	m
$w(\theta_i)$	Lorentzian width as a function of angle of incidence for pseudo-specular reflected rays	radians
ω	Rotational angle around specular direction	radians
W	Width of light extractor	m
Ω_{lc}	Solid angle enclosed by a single critical loss cone	steradians
Ω_e	Solid angle enclosed by endlight (escaping light) at collection edge	steradians
$\Delta\Omega_{det}$	Solid angle of detector in photogoniometer	steradians